Drag reduction in turbulent channel flow by phase randomization

R. A. Handler
Naval Research Laboratory, Washington, D.C. 20375

E. Levich[a]
Department of Physics, City College of CUNY, New York, New York 10031

L. Sirovich
Department of Mathematics, Brown University, Providence, Rhode Island 02912

Results of numerical simulations of plane turbulent channel flow are presented in which a forcing is introduced which derives from the randomization of selected Fourier modes. In all cases, the randomization is introduced uniformly throughout the channel. The properties of the resulting turbulence are strongly dependent on both the wave numbers whose phases are randomized and the forcing frequency. Two principal wave-number bands have been selected. The first includes a selected subset of the largest length scales of the turbulence. Forcing in this band results in a fully sustained maximum mass flux increase above that of normal turbulence of 30%, which translates into a drag reduction of 58%. Many of the statistical properties of the simulated drag-reduced turbulence generated in this manner are in good qualitative agreement with the statistical properties of turbulence observed in experiments in which drag reduction is achieved through the introduction of small concentrations of long-chained polymers into the flow. In a second set of simulations, the phases of the intermediate and smallest wavelengths were randomized. Forcing at these scales of motion results in a drag increase. Speculations on the mechanism of the drag reduction by phase randomization are offered.

I. INTRODUCTION

In this paper we demonstrate, by direct numerical simulation, that a significant drag reduction can be obtained in turbulent channel flow by introducing a periodic randomization of the phases of selected Fourier modes of the velocity field. Motivation for the current investigation is due in part to the recent discovery[1,2] of propagating modes in turbulent channel flow, and to prior random phase calculations in homogeneous[3,4] turbulence. In the work cited above, it was determined that the interaction of the wavelike modes with streamwise oriented *roll* modes generate a significant fraction of the bursting activity in channel flow turbulence. The roll modes themselves, which represent streamwise oriented vortices, are found to contain a large fraction of the turbulent energy that is released during bursting events.

These observations prompted us to determine the length and time scales of the turbulence which may be most important in determining turbulence production and the subsequent generation of drag. That is, we seek to determine if the perturbation of the wavelike modes can produce significant changes in the turbulence. Here we use the method of phase randomization, to be described below, which allows for the selective perturbation of the turbulence in a manner which does no work on the flow. We indicate below that a randomization of the phases of selected Fourier components of the velocity field is equivalent to a velocity-dependent forcing in physical space. This

forcing in no way violates the fundamental governing equations. A further objective here is to give guidance to experimentalists who seek new methods of modification and control of turbulence rather than to suggest specific physical experiments. In this sense, no matter what method is chosen to perturb the turbulence (i.e., wall movement, acoustic excitation, suction, or blowing), knowledge of the length and time scales which are active in generating drag is of critical importance.

An unexpected result of our work is that a phase randomization of the wavelike modes produces drag-reduced turbulence with many of the characteristics observed in experiments[5,6] in which drag reduction is produced by introducing small concentrations of high molecular weight polymer into the flow. We describe below the similarities and some differences between the phase-randomized turbulence and the polymer case. We emphasize that even though the similarities between these two cases are remarkably close, we in no way imply that the physical mechanism(s) by which polymers reduce drag are the same as in the phase-randomized case. Nevertheless, given the lack of a complete understanding of polymer-induced drag reduction, which is reflected in the existence of several competing theories, we maintain that a direct comparison between the polymer case and the forced turbulence may lead to a better understanding of both. Our intent here is not to imply that polymers literally randomize the phase of selected wavelike modes but that some form of *analogy* between the two cannot be ruled out. In any case, the striking similarities between these two cases warrants a comparison which we give in Sec. IV.

[a]Present address: ORMAT Turbines Ltd., New Industrial Area, P.O. Box 68, Yavne 70650, Israel.

II. NUMERICAL METHODS

We have performed direct numerical simulations of turbulence in a periodic channel with rigid no-slip walls. Following earlier treatments[7,8] a fully spectral code is used, in which the velocity field is approximated by Fourier modes in the streamwise (x) and spanwise (z) directions and Chebyshev polynomials in the wall-normal (y) direction. In the present instance the turbulent flow is driven by a constant streamwise pressure gradient. For all simulations reported here we have used $65 \times 64 \times 48$ grid points in the y, z, and x directions, respectively. The channel dimensions are $L_y = 2h$, $L_z = 5h$, and $L_x = 10h$, where h is the channel half-width. In our simulations, the velocity field $\mathbf{u} = (u, v, w)$ where u, v, w are the streamwise, wall normal, and spanwise components, respectively, is given by

$$\mathbf{u}(\mathbf{x},t) = \sum_{n=-N/2}^{N/2-1} \sum_{m=-M/2}^{M/2-1} \sum_{p=0}^{P} \mathbf{a}_{nmp} T_p(y) e^{i(k_n x + k_m z)}, \tag{1}$$

where $T_p(y)$ denotes the Chebyshev polynomials, and the wave numbers are defined by $k_n = 2\pi n/L_x$ and $k_m = 2\pi m/L_z$.

The effect of the above-mentioned phase randomization is equivalent to a forcing term in the Navier–Stokes equations as follows:

$$\rho \frac{D\mathbf{u}}{Dt} + \nabla p - \mu \nabla^2 \mathbf{u} = \sum_n \mathbf{F}_n[\mathbf{u}] \delta(t - t_n), \tag{2}$$

where ρ is the density and μ is the viscosity. In addition we enforce the incompressibility constraint:

$$\nabla \cdot \mathbf{u} = 0, \tag{3}$$

and the boundary conditions

$$\mathbf{u} = 0, \quad y/h = \pm 1. \tag{4}$$

Several forms for the function $\mathbf{F}_n[\mathbf{u}]$ were used and in all cases the force is workless

$$\mathbf{F}_n \cdot \mathbf{u} = 0. \tag{5}$$

For the cases reported on here selected coefficients $\mathbf{a}_{nmp}$, at the discrete times, t_n, were given a random phase shift,

$$\mathbf{a}_{nmp} \rightarrow e^{i\phi_{nm}} \mathbf{a}_{nmp}, \tag{6}$$

where ϕ_{nm} is independent of y. Kinematical consistency requires that the transformation (6) be applied to the vorticity field simultaneously. Clearly (6) preserves continuity and shifts the turbulent eddies or waves with respect to each other without in any way changing the energy of the flow. The no-slip boundary conditions (4) are also preserved by (6). Although the times, t_n, were chosen to be uniform this is unnecessary and a *shot-noise* distribution of intervals should not change our results. The workless nature of the forcing described in (2) has been emphasized only to underline the fact that the forcing is nonintrusive. More intrusive forcing mechanisms, some of which have been mentioned in the Introduction, may in fact be equally effective. In fact, two experiments based on the results of these simulations are now in progress. One uses acoustic excitation and the other vibrating ribbons to achieve the desired forcing.

Before applying random phasing we integrated forward in time until a steady state was established. This was shown to satisfy the averaged form of the streamwise momentum equation for statistically steady turbulence:

$$\frac{y}{h} = \frac{\overline{uv}}{u^{*2}} - \frac{v}{u^{*2}} \frac{d\bar{U}}{dy}. \tag{7}$$

Since the right-hand side of (2) averages to zero (7) remains valid. Here, $y = 0$ is the channel centerline, $u^* = \sqrt{\tau_w/\rho}$ is the friction velocity, τ_w is the wall shear stress, v is the kinematic viscosity, $\bar{U}$ is the mean velocity, and $\overline{uv}$ is the Reynolds stress. Equation (7) was verified by averaging the flow over a time interval $\Delta T u^{*2}/v = \Delta T^+ = 4687$. We estimate that for this flow the large eddy turnover time, T_e, is measured by $2h/u'$ where u' is a typical root mean square fluctuation level. The magnitude of the peak streamwise velocity fluctuation, u'/u^*, is about 2.6 and for our flow, the driving pressure gradient is chosen so as to achieve a friction Reynolds number, $R^* = u^* h/v$, of 125. These values give $T_e u^{*2}/v = T_e^+ = 96$ so that the ratio of total run time to the eddy turnover time for this simulation, which we refer to as *normal* turbulence, is about 50. Once we have established a steady-state turbulence in this way the phase randomizations are turned on.

III. RESULTS: LOW-WAVE-NUMBER PHASE RANDOMIZATION

For the first set of simulations we apply phase randomization only to the band of low-wave-number modes for which

$$1 \leqslant n \leqslant 11; \quad |m| \leqslant 6.$$

This band represents, approximately, an isotropic randomization such that

$$\sqrt{k_n^2 + k_m^2} \leqslant k_{max}/6,$$

where $k_{max} = 32 \times (2\pi/L_z)$ is the largest wave number in the simulation. In doing this the intention is to interfere, and produce incoherence in the propagating modes which have been shown to trigger the bursting events that are at the heart of drag production. The streamwise homogeneous modes, $n = 0$, $|m| \leqslant 6$ are excluded since these modes, referred to as kinematically degenerate modes, do not propagate. In fact these modes correspond to the streamwise rolls or streaks.[9,10] The result of including the roll modes and further discussion appears in the following sections. Five simulations for this wave-number band have been performed (runs LK1–LK5).

In each run, the time interval between phase randomizations, $\Delta T_r^+ = \Delta T_r u^{*2}/v$, where ΔT_r is the time interval between phase randomizations in computational units, has been changed; ΔT_r^+ was varied from 4.69 to 23.44, where $\Delta T_r^+ = 4.69$ represents 60 computational time steps. A summary of these and other results is given in Table I.

TABLE I. Summary of global properties for all simulations.

Run	ΔT^+	ΔT_r^+	$\overline{R_b}$	$\overline{R^*}$	$\overline{R_b}/R_b^0$	DR(%)
Normal turbulence	4 687	∞	1850	125.0	1.0	0.0
LK1	10 156	4.69	2353	124.9	1.27	+52
LK2	10 156	9.38	2414	127.2	1.30	+58
LK3	10 156	14.06	2244	125.7	1.21	+40
LK4	10 156	18.75	2153	125.0	1.16	+30
LK5	10 156	23.44	2030	124.3	1.10	+18
LK0	5 078	4.69	1953	124.5	1.06	+11
N0	5 078	4.69	1829	123.0	0.99	−2
HK1	5 078	4.69	1760	124.4	0.95	−9
HK2	5 078	23.44	1831	125.2	0.99	−2
HK3	5 078	4.69	1921	126.0	1.04	+7
Laminar flow			5208	125.0	2.74	+483

Each simulation was run for 130 000 time steps which corresponds to $\Delta T^+ = 10$ 156, and took approximately 45 h on a Cray-YMP. Each run represents approximately 100 large eddy turnover times, and, for example, run LK1 represents 2160 phase randomizations. Complete realizations of the velocity field were stored every 3250 time steps. For each simulation we have used identically the same initial condition which is taken to be a fully developed realization of the normal turbulence simulation mentioned above.

In Fig. 1 we display, for run LK1, the dependence of the mass flux Reynolds number, $R_b = U_b h/\nu$ [where $U_b = 1/2h \int_0^{2h} \bar{U}(y) dy$] and R^* versus time, $T^+ = t u^{*2}/\nu$, where t is the computational time. It is evident that, immediately after turning on the phase randomization, the

drag drops rapidly, as indicated by the results for R^*, and reaches a minimum value in about ten large eddy turnover times. Since the flow is driven by a constant pressure gradient, it must achieve the same value of $R^* = 125$ that it will achieve had there been no random forcing. Figure 1(b) traces the recovery of R^* back to its expected value. The mass flux Reynolds number increases sharply during the period of reduced drag. This is expected since during this time interval there is an imbalance between the driving pressure gradient and the wall shear leading to an acceleration of the flow. From Fig. 1(a) it appears that the steady-state mass flux for run LK1 is substantially higher than the steady-state mass flux for normal turbulence. The flow in this case reaches nearly a statistically steady state at about $T^+ = 4000$. The data obtained subsequent to this time (which differs from case to case) is used in all runs to determine all turbulence statistics which we present in this paper. In all runs we have verified that the flow is statistically steady by determining that (7) is satisfied to within 3% in all cases.

In Table I we summarize the overall properties of the flow in each simulation. In run LK1 we note that $\overline{R_b}$, where the overbar denotes averaging only during the steady state, is 27% larger than in normal turbulence, whose mass flux Reynolds number, $R_b^0 = 1850$. (We note that the experimental correlation of Dean[11] predicts $R_b^0 = 1824$ for normal turbulence which is in good agreement with our result.) It is also possible to estimate the drag reduction,

$$\text{DR} = (\tau_1 - \tau_0)/\tau_0,$$

where τ_1 is an estimate of the wall shear stress for normal turbulence with the mass flux in the *simulated* flow, and τ_0 is the wall shear for normal turbulence. (From Dean[11] we have $\tau \propto U_b^{7/4}$.) For run LK1, the drag reduction is 52% on this basis. Results for R_b and R^* for run LK5, for which the randomization time is $\Delta T_r^+ = 23.44$, are shown in Fig. 2 and Table I. It is evident that in this case the drag rebound, after the initial drag decrease, is somewhat stronger than for run LK1. It is also apparent that the fluctuations in both R_b and R^* are both larger in amplitude and larger in time scale than for run LK1. In this case the mass flux increase is 10% and the corresponding drag reduction is
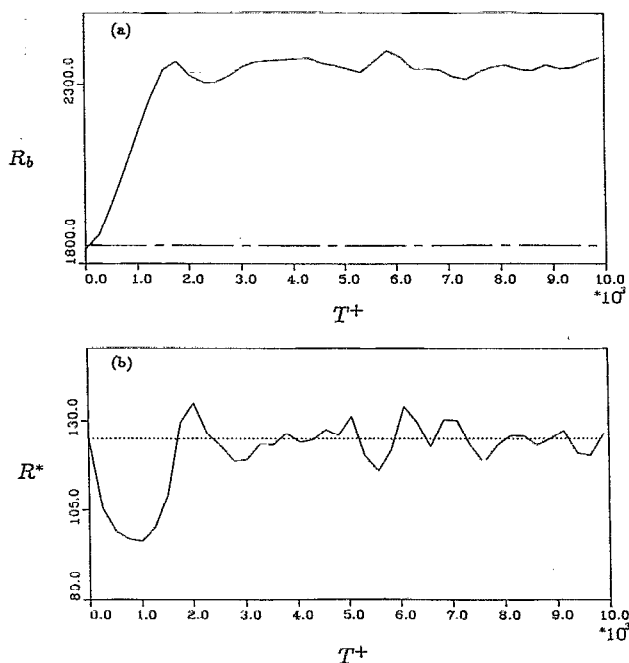

FIG. 1. Mass flux and friction Reynolds numbers versus time for drag reduced turbulence. Results are for $\Delta T_r^+ = 4.69$ (run LK1). (a) R_b vs T^+; steady-state result for normal turbulence, $R_b = 1850$ (– – –). (b) R^* vs T^+; steady-state result for constant pressure gradient turbulence, $R^* = 125$ (···).
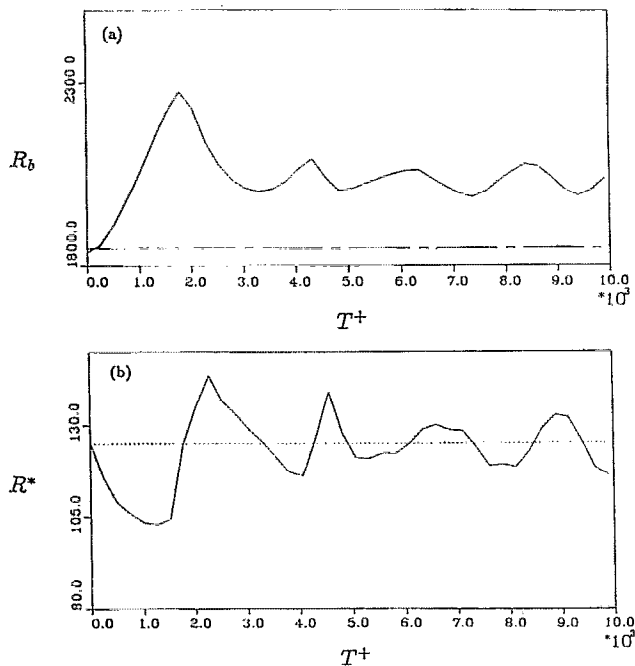
FIG. 2. Mass flux and friction Reynolds numbers versus time for drag reduced turbulence. Results are for $\Delta T_r^+ = 23.44$ (run LK5). (a) R_b vs T^+; steady-state result for normal turbulence, $R_b = 1850$ (– – –). (b) R^* vs T^+; steady-state result for constant pressure gradient turbulence, $R^* = 125$ ($\cdots$).

18%. These results clearly demonstrate that a substantial fully sustained drag reduction can be obtained by a phase randomization of a relatively small subset of the available Fourier modes and that the active modes are the ones representing the largest length scales, excluding, as mentioned above, the longest streamwise modes. Furthermore, the largest drag reduction obtained in this manner (58% in run LK2) is comparable to the percent drag reduction observed experimentally[5,6] which can be on the order of 60% for the largest polymer concentrations. We note that these drag reductions have been achieved without in any way attempting to optimize the effect except insofar as we have varied ΔT_r^+ and the wave-number band in which the random force acts.

IV. COMPARISON WITH POLYMER ADDITIVE DRAG REDUCTION

It is of interest to compare the details of the turbulence statistics we have obtained with those obtained from polymer drag-reduced flows. Before proceeding, we caution that although our results resemble, in many respects, the kind of turbulence observed experimentally in polymer flows, certain differences do exist. These differences, which will be pointed out below, indicate to us that the mechanism of drag reduction obtained by phase randomization is likely to differ in certain respects from the polymer mechanism. It is difficult to compare our results *directly* with those from polymer experiments for several reasons. First, the more recent experiments[12,13] were performed at Rey-

nolds numbers that were five times larger than our direct simulations. Second, it is not possible at the present time to determine the correspondence, if any, between the randomization frequency in our simulations and the polymer concentration. Finally, it may be the case that many drag-reduced flows have common statistical features. (On the other hand, a recent numerical simulation[14] shows that this is not always true.) If this is the case, then our simulations provide a range of new statistical measures for such drag-reduced flows. As an aid in making such a comparison we briefly summarize the more widely accepted polymer-induced effects on turbulence statistics and structure.

The introduction of polymers increases the size of the buffer layer of the turbulent mean velocity profile which exists in normal turbulence in the region $5 \leqslant y^+ \leqslant 30$, where $y^+ = yu^*/\nu$. The logarithmic layer, which exists in our normal turbulence calculation in the region $30 \leqslant y^+ \leqslant 100$, and which obeys the law $\bar{U}^+ = 1/\kappa \ln(y^+) + B$ where κ is von Kármán's constant, and $\bar{U}^+ = \bar{U}/u^*$, is preserved in drag-reduced polymer turbulence. It has been conjectured[5,6] that the persistence of the log layer in the polymer case is evidence that the polymers have no significant effect on the energy containing eddies. Experiments[15] suggest that drag reduction is induced only when polymer molecules are injected into the buffer layer, though recently it has been found, and apparently now disputed, that drag reduction may also occur with injection only at the centerline.[16–18] It is clear,[19] however, that no drag reduction occurs when the polymer is confined to the sublayer ($y^+ \leqslant 5$). Experiments[12,13] also indicate that the peak value of u', the root mean square value of the streamwise velocity component, is larger in polymer turbulence compared to Newtonian turbulence. Also, this peak value is located farther from the wall in the polymer case. The wall-normal component, v', has been found to be damped[12,13] throughout the flow and w' is reduced near the wall.[20] It has also been established[12,13] that $\overline{uv}$ is reduced in polymer turbulence and the position of its peak value shifts farther from the wall.

In Fig. 3 we plot $\bar{U}^+$ for simulations LK1–LK5. It is evident that phase randomization, in agreement with the polymer case, enlarges the buffer layer. In contrast to experiments, however, the logaritmic layer appears to have been eliminated in our simulations. We recall that in the polymer case, however, the logarithmic layer persists. However, for our normal turbulence calculation, the logarithmic layer is seen to be of limited spatial extent as a result of the relatively low Reynolds number of the simulation. Thus it would be premature to attach any significance to this feature of the calculation. Clarification of this issue must await simulations at higher Reynolds numbers where we can expect a larger and more clearly defined logarithmic layer.

In Fig. 4 we show the turbulence intensity profiles for runs LK1 and LK5. It is evident in both cases, that the peak value of u' is significantly larger than in normal turbulence and also that its distance from the wall has increased. These results are clearly consistent with results for polymer flows. For run LK5 we find that both v' and w'
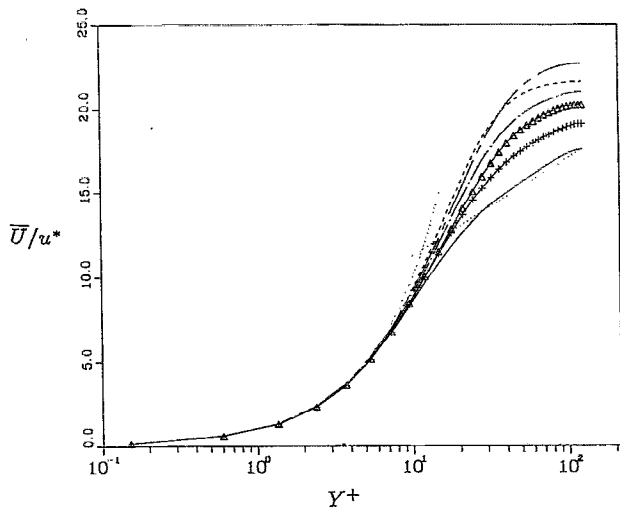
FIG. 3. Mean velocity profiles. Steady-state profile for normal turbulence simulation (——). Steady-state profile for $\Delta T_r^+ = 4.69$ (– – –). Steady-state profile for $\Delta T_r^+ = 9.38$ (- - -). Steady-state profile for $\Delta T_r^+ = 14.06$ (– · –). Steady-state profile for $\Delta T_r^+ = 18.75$ ($\triangle$). Steady-state profile for $\Delta T_r^+ = 23.44$ (+). Law of the wall, $\bar{U}/u^* = 2.5 \, \ln(y^+) + 5.5$ and $\bar{U}/u^* = y^+$ (···). (The results shown here and in subsequent figures were obtained by averaging data from both sides of the channel.)

are significantly reduced throughout the entire domain, which is also in harmony with known polymer results. For the intermediate cases, LK2–LK4, the intensity profiles are all qualitatively similar to run LK5. In run LK1, the case corresponding to the highest forcing frequency, it is evident that the peak values for v' and w' occur at the channel centerline and are well above normal turbulence levels there. Of the five simulations, run LK1 is the only one which gives v' results that differ qualitatively from polymer results. In Fig. 5 results for the Reynolds stress and the turbulence production, $\overline{uv}(d\bar{U}/dy)$, for both runs LK1 and LK5 are shown. In both cases, $\overline{uv}$ is reduced and the location of its peak shifts from the wall to the core region which is consistent with the previously cited experimental results. It should be observed that in the case of polymer additives Eq. (5) is replaced by

$$-\frac{\overline{uv}}{u^{*2}} + \frac{\nu}{u^{*2}} \frac{d\bar{U}}{dy} = -\frac{y}{h} \frac{\bar{\tau}_e}{\rho u^{*2}}, \qquad (8)$$

where τ_e represents the stress contribution from the viscoelastic effect. As noted above, our results obey (7), whereas in the polymer case the additional stress τ_e is significant.[13] It is also apparent that phase randomization reduces the peak value of the production and shifts it farther from the wall. Recent experiments[21] clearly indicate the shift away from the wall but only a weak decrease in the peak value of the production. The experiments do show, however, a reduction in the channel-average production of u.
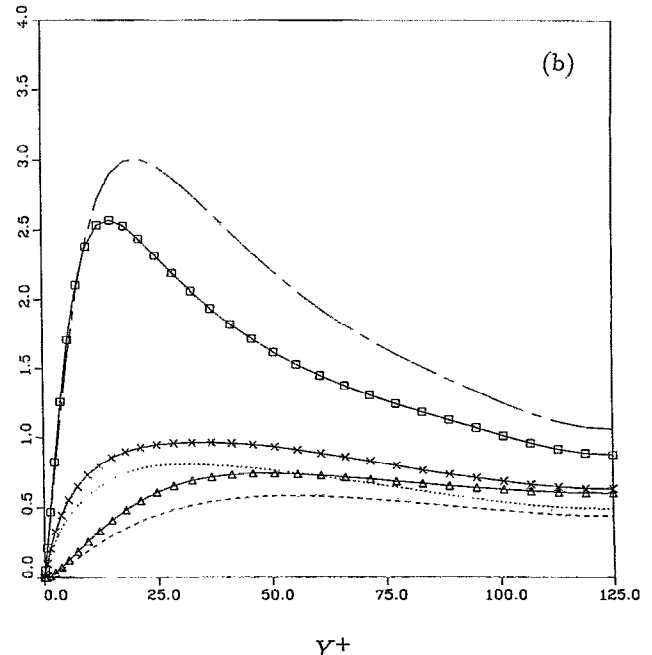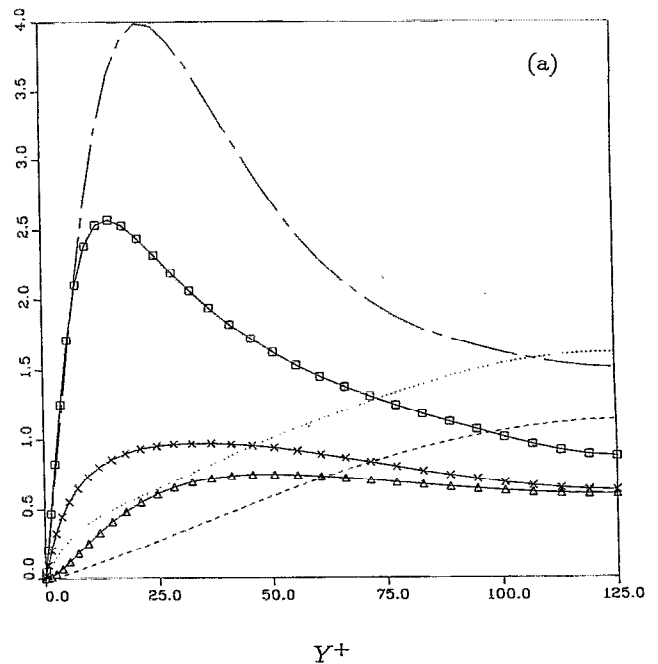

FIG. 4. Root mean square turbulence statistics. (a) Run LK1, $\Delta T_r^+ = 4.69$; (b) run LK5, $\Delta T_r^+ = 23.44$. Normal turbulence: u'/u^* ($\square$); v'/u^* ($\triangle$); w'/u^* ($\times$). Drag-reduced turbulence simulation: u'/u^* (– – –); v'/u^* (- - -); w'/u^* (···).

V. FURTHER RESULTS

In Fig. 6 the time history of the mass flux Reynolds number is shown for all runs. A particularly interesting behavior is noted in runs LK2, LK3, and LK4. In these cases, the initial rise in the mass flux is sustained for a remarkably long time period (on the order of 4700 viscous times for run LK2) before decreasing rapidly as the flow
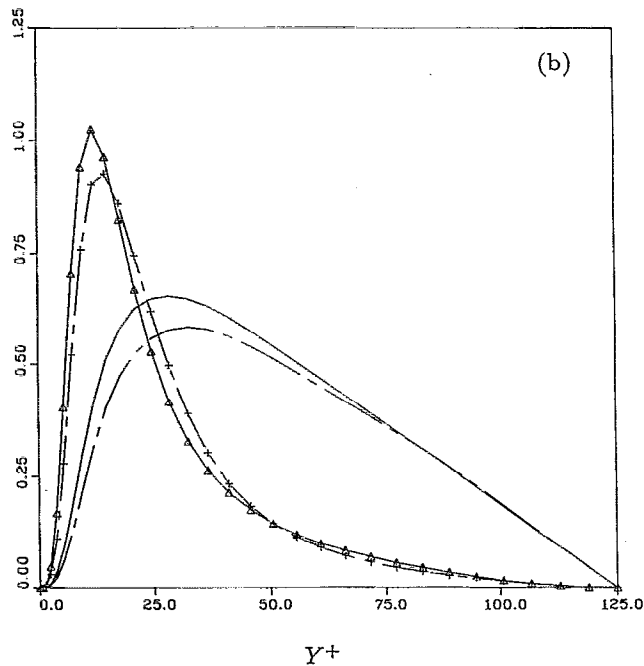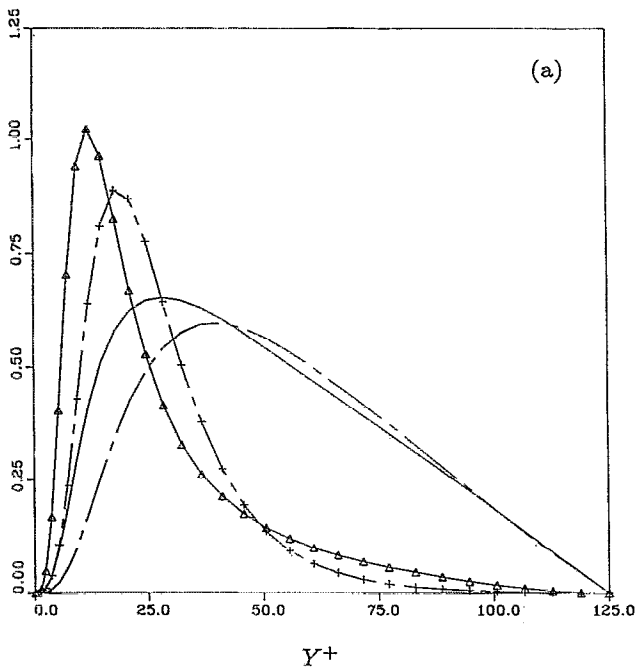
FIG. 6. Mass flux Reynolds number versus time for all simulations. $\Delta T_r^+ = 4.69$ (run LK1):——; $\Delta T_r^+ = 9.38$ (run LK2):$\cdots$; $\Delta T_r^+ = 14.06$ (run LK3):---; $\Delta T_r^+ = 18.75$ (run LK4):- $\cdot$ -; $\Delta T_r^+ = 23.44$ (run LK5):- - -; $\Delta T_r^+ = 4.69$ (run LK0): $\triangle$; $\Delta T_r^+ = 4.69$ (run HK1): $+$; $\Delta T_r^+ = 23.44$ (run HK2): $\times$; $\Delta T_r^+ = 4.69$ (run HK3): $\Diamond$; $\Delta T_r^+ = 4.69$ (run N0): ∇; steady-state result for normal turbulence, $R_b = 1850$: $\boxtimes$.

FIG. 5. Reynolds stress and turbulence production of the streamwise velocity component. (a) Run LK1, $\Delta T_r^+ = 4.69$; (b) run LK5, $\Delta T_r^+ = 23.44$. Reynolds stress, $\overline{uv}/u^{*2}$; normal turbulence (——); drag-reduced turbulence (- - -). Turbulence production, $5 \times \overline{uv}(d\bar{U}/dy)$ $\times (\nu/u^{*4})$; normal turbulence ($\triangle$); drag-reduced turbulence simulation ($+$).

that R^* remains well below its steady-state value until, at $t^+ \simeq 4500$, it rapidly rises to a peak in only a few hundred viscous time units. We have found that during the period in which R^* is near its minimum value, v', w', and $\overline{uv}$ are approximately one order of magnitude smaller than in normal turbulence, though u' is near normal levels. This be-

approaches a statistically steady state. We also note that the peak value of R_b in runs LK2 and LK3 is quite high ($\simeq 3300$) when we consider that for the same pressure gradient $R_b = 5208$ for laminar flow. Further understanding of this phenomenon is achieved by referring to Fig. 7 where we plot R^* versus time for run LK2. It is evident
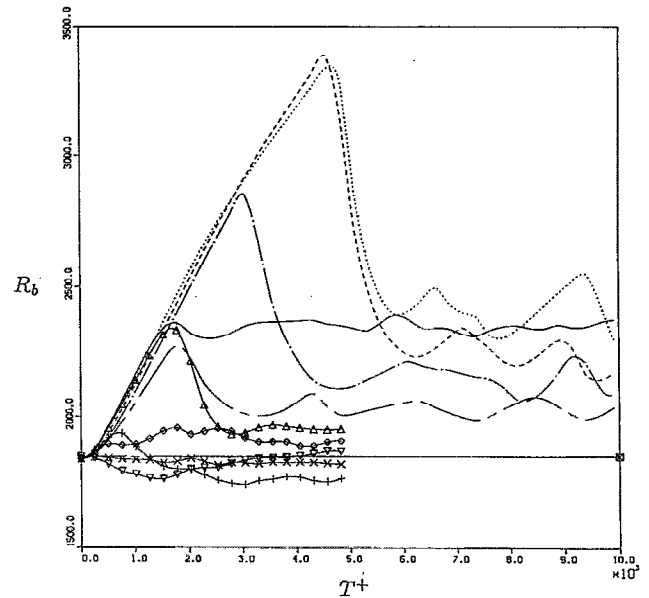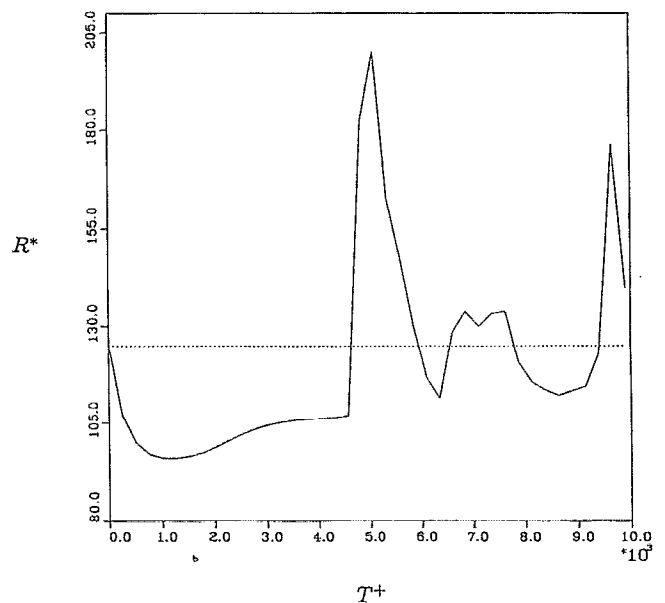

FIG. 7. Friction Reynolds number versus time for run LK2. Steady-state result for normal turbulence, $R^* = 125$ ($\cdots$).

havior leads us to conjecture that the flow is in fact relaminarizing. The subsequent rise in wall shear and rapid drop in mass flux indicates that the flow is undergoing a transition back to a fully turbulent state. Subsequent to this transition the flow approaches a steady state though we appear to observe another weaker transition toward the end of run LK2.

We have also performed one calculation (run LK0) in which we have *included* the kinematically degenerate modes (i.e., the modes for which $n=0$), in the randomization scheme. Here we randomize in the region $0 \leqslant n < 11$, $|m| \leqslant 6$ where we have included the modes for which $n=0$. Run LK0 differs only in this respect from run LK1. It is evident in Fig. 6 that inclusion of these modes reduces the drag reduction dramatically from 52% in LK1 to 11% in LK0. The modes for which $n=0$ are the principal energy bearing modes of the fluctuating flow field.[1,2,22] As observed earlier they correspond to the *rolls* or *streaks* that have been observed in experiments. An accepted scenario for the drag producing bursting and sweeping events is that these rolls lift up, and somewhat violently, as hairpins (or parts of hairpins), thereby injecting slow moving fluid into the free stream and inducing high momentum fluid to move to the boundaries. These simulations give some support to this view. Perturbing the modes for which $n=0$ destroys the coherence of rolls and it is our contention that this enhances the ejection process—hence decreasing the drag reducing effect of randomizing the wavelike modes alone. This, however, cannot be considered a complete explanation for this effect since, when only the roll modes ($n=0$, $|m| \leqslant 6$) are randomized in run N0, only a small drag increase of 2% is obtained.

In runs HK1 and HK2 we randomize only the intermediate and high wave numbers in the region $11 \leqslant n \leqslant 24$, $|m| \leqslant 32$; $0 \leqslant n < 11$, $5 < |m| \leqslant 32$. This region is essentially a direct complement of the region used in runs LK1–LK5 and represents, approximately, the isotropic region $|\mathbf{k}| > k_{max}/6$. (In run HK3 we *did not* randomize the modes $n=0$, $5 < |m| \leqslant 32$ in the region described above. For this run we achieve a drag reduction of 7%.) It is evident from Fig. 6 and Table I that randomization of these modes actually leads to a *drag increase* of 9% in HK1 and 2% in HK2. It is apparent that we can achieve a significant drag reduction only by perturbing the energy containing region of the spectrum.

In Fig. 8 we summarize our drag reduction results by plotting the steady-state mass flux Reynolds number against randomization frequency for all runs. For runs LK1–LK5 we have placed a best-fit curve through the data. It is clear that as $\Delta T_r^+ \to \infty$, that $\overline{R_b} \to 1850$, the steady-state value for normal turbulence, since in this limit the turbulence has time to relax to its normal state between randomizations. For $\Delta T_r^+ \to 0$ we expect $\overline{R_b} \to 1850$ again, since the point at $\Delta T_r^+ = 0$ represents a randomization at every time step and the flow could not evolve from its initial condition. From this argument we should expect some value of ΔT_r^+ for which the mass flux is a maximum and for our simulations this appears to be at $\Delta T_r^+ \simeq 7$. We mention in passing that Lumley[5,6] estimates the time scale
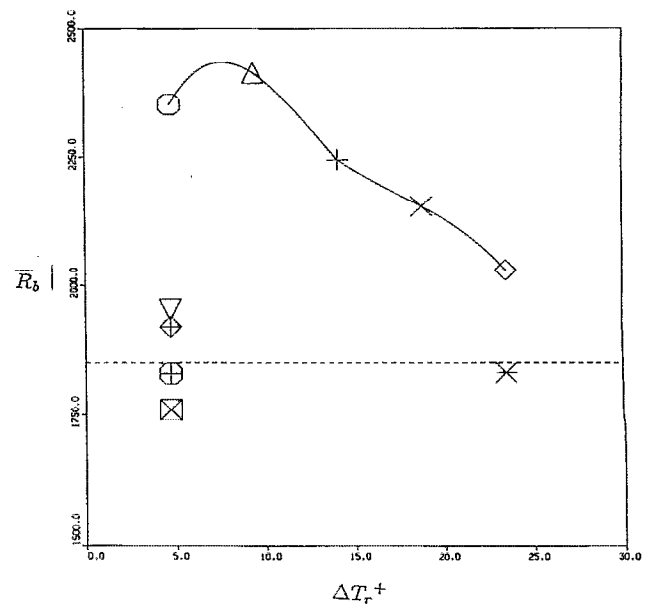

FIG. 8. Steady-state mass flux Reynolds number versus randomization frequency. Run LK1 ($\bigcirc$); run LK2 ($\triangle$); run LK3 ($+$); run LK4 ($\times$); run LK5 ($\Diamond$); run LK0 (∇); run HK1 ($\boxtimes$); run HK2 (*); run HK3 (ϕ); run N0 ($\oplus$). Steady-state result for normal turbulence, $R_b = 1850$ (---). (See also Table I.)

for the flow at maximum dissipation to be $\Delta T_r^+ \simeq 10$ and uses this to argue in favor of a time scale theory for polymer drag reduction. The agreement between our time scale for maximum drag reduction and the Lumley time scale may not be coincidental though we cannot justify this conjecture at this time.
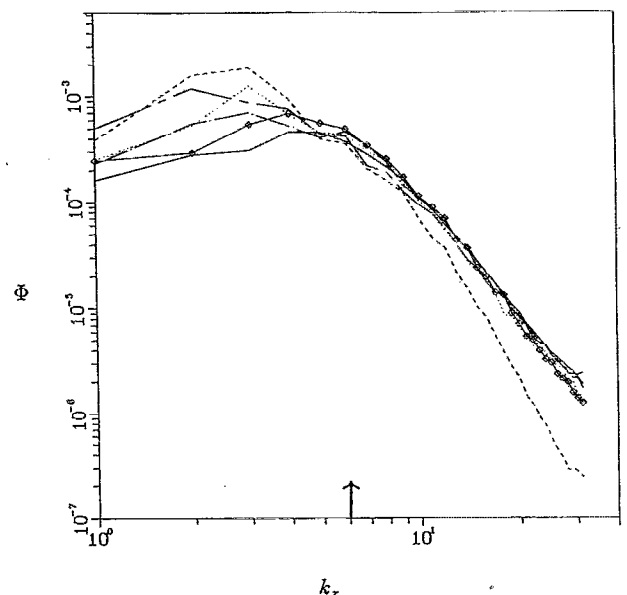

FIG. 9. Spanwise wave-number spectrum for the streamwise component of velocity at $y+ = 14.8$. Normal turbulence simulation (——); run LK1 (---); run LK2 (– – –); run LK3 ($\cdots$); run LK4 (– · –); run LK5 ($\Diamond$). Arrow indicates wave number below which modes are randomized.

Finally, we present results for the energy spectra for runs LK1–LK5 in Fig. 9. The spanwise spectra, $\Phi(k_z)$, at $y^+ = 14.7$ for the streamwise component of velocity are shown. We choose to examine this particular spectrum since it is well known that near the wall ($y^+ \approx 15$) a streaky structure with a spanwise wavelength of about $100\nu/u^*$ is evident in flow visualizations and is also evident as a peak in the spanwise spectrum at the appropriate wave number. This peak is evident in the spectrum for normal turbulence shown in Fig. 9. Below the cutoff wave number (i.e., the wave number below which randomization is employed) the spectra for all cases show a significant increase in energy and a clear shift in their peak values toward lower wave numbers. This suggests that the spanwise wavelength of the *roll* modes which produce the streaks have become larger. Interestingly, in the polymer case[23] this is also observed. With the exception of run LK1 it is evident that, above the cutoff wave number, all spectra appear to collapse onto the normal turbulence spectrum. This result is of some significance since we have apparently achieved significant drag reductions without affecting the small-scale structure of the turbulence and apparently leaving the basic Kolmogorov cascade unaffected. In polymer experiments,[24] however, there appears to be a damping of small-scale structure in addition to the increased energy of the large scales which we observe. We note, however, that in runs HK1 and HK2, where only the small scales were randomized, we have observed a strong damping of the small-scale structures *above* the cutoff wave number and little change in energy below it.

VI. CONCLUSIONS

We have determined that phase randomization of a relatively small subset of the available Fourier modes in channel flow turbulence gives rise to a fully sustained drag reduction of about the same magnitude as found in the polymer case. We have pointed out many similarities and some differences between these two cases which lead us to speculate on a mechanism for drag reduction by phase randomization. In one theory that has been proposed to explain polymer-induced drag reduction[5,6] (although alternate theories exist[25,26]), the polymers induce a higher effective viscosity in the bulk of the flow which drives the peak in the dissipation spectrum to smaller wave numbers (larger length scales). The energy containing scales are assumed to remain unchanged. As a result, the distance above the wall at which the turbulence can be self-sustaining through an energy cascade becomes larger. Consequently, the mean shear at the wall decreases under the assumption that the viscosity in the sublayer remains unchanged.

In our simulations, the relatively small log layer disappears and there is a lack of significant changes in the dissipation scales. Thus drag reduction due to phase randomization may be due to a different mechanism. We speculate, in view of the recent discovery of plane waves[1,2] in turbulent channel flow, that phase randomization leading to drag reduction may be destroying the coherence of the turbulence producing structures near the wall. The so-called bursting mechanism may be inhibited by a phase randomization of the wavelike modes. In future investigations we hope to clarify the mechanism of drag reduction described in this work by localizing the randomization. For example, we may perform simulations in which only the region near the wall is forced in the manner described above. In addition, we are now performing physical experiments in which acoustic excitation and vibrating ribbons will be used to perturb the turbulence at the length and time scales identified by these numerical simulations.

[1] L. Sirovich, K. S. Ball, and L. R. Keefe, "Plane waves and structures in turbulent channel flow," Phys. Fluids A **2**, 12 (1990).
[2] L. Sirovich, K. S. Ball, and R. A. Handler, "Propagating structures in wall-bounded turbulent flows," Theor. Comput. Fluid Dyn. **2**, 307 (1991).
[3] E. Levich, L. Shtilman, and A. V. Tur, "The origin of coherence in hydrodynamical turbulence," Physica A **176**, 241 (1991).
[4] Y. Murakami, L. Shtilman, and E. Levich, "Reducing turbulence by phase juggling," Phys. Fluids A **4**, 1776 (1992).
[5] J. L. Lumley, "Drag reduction by additives," Annu. Rev. Fluid Mech. **1**, 367 (1969).
[6] J. L. Lumley, "Drag reduction in turbulent flow by polymer additives," J. Polymer Sci. Macromol. Rev. **7**, 263 (1973).
[7] J. Kim, P. Moin, and R. Moser, "Turbulence statistics in fully developed channel flow," J. Fluid Mech. **177**, 133 (1987).
[8] R. A. Handler, E. W. Hendricks, and R. I. Leighton, "Low Reynolds number calculation of turbulent channel flow: A general discussion," Naval Research Laboratory Memorandum Report 6410, 1989.
[9] J. M. Wallace, R. S. Brodkey, and H. Eckelmann, "Pattern-recognized structures in bounded turbulent shear flows," J. Fluid Mech. **83**, 673 (1977).
[10] R. F. Blackwelder and R. E. Kaplan, "On the wall structure of the turbulent boundary layer," J. Fluid Mech. **76**, 89 (1976).
[11] R. Dean, "Reynolds number dependence of skin friction and other bulk flow quantities in two-dimensional rectangular duct flow," Trans. ASME I: J. Fluids Eng. **100**, 215 (1978).
[12] T. Luchik and W. Tiederman, "Turbulent structure in low-concentration drag-reducing channel flows," J. Fluid Mech. **190**, 241 (1988).
[13] W. Willmarth, T. Wei, and C. Lee, "Laser anemometer measurements of Reynolds stress in a turbulent channel flow with drag reducing polymer additives," Phys. Fluids **30**, 933 (1987).
[14] W. Jung, N. Mangiavacchi, and R. Akhavan, "Suppression of turbulence in wall-bounded flows by high-frequency spanwise oscillations," Phys. Fluids A **4**, 1605 (1992).
[15] W. McComb and L. Rabie, "Local drag reduction due to injection of polymer solutions into turbulent flow in a pipe. Part 1: Dependence on local polymer concentration; Part 2: Laser-Doppler measurements of turbulent structure," AIChE J. **28**, 547 (1982).
[16] W. McComb and L. Rabie, "Development of local turbulent drag reduction due to nonuniform polymer concentration," Phys. Fluids **22**, 183 (1979).
[17] H. W. Bewersdorff, "Effect of centrally injected polymer thread on drag in pipe flow," Rheol. Acta **21**, 587 (1982).
[18] H. W. Bewersdorff, "Heterogene widerstrandsverminderung bei turbulenten rohstromungen," Rheol. Acta **23**, 522 (1984).

[19] W. Tiederman, T. Luchik, and D. Bogard, "Wall-layer structure and drag reduction," J. Fluid Mech. **156**, 419 (1985).

[20] M. J. Rudd, "Velocity measurements made with a laser Dopplermeter on the turbulent pipe flow of a dilute polymer solution," J. Fluid Mech. **51**, 673 (1972).

[21] K. Harder and W. Tiederman, "Influence of wall strain rate, polymer concentration, and channel height upon drag reduction and turbulent structure," ONR Contractor Report PME-FM-89-1, 1989.

[22] P. Moin and R. D. Moser, "Characteristic eddy decomposition of turbulence in a channel," J. Fluid Mech. **200**, 471 (1989).

[23] L. Eckelman, G. Fortuna, and T. J. Hanratty, "Drag reduction and wavelength of flow-oriented wall eddies," Nature **236**, 94 (1972).

[24] C. Berner and O. Scrivner, "Drag reduction and structure of turbulence in dilute polymer solutions," in *Viscous Flow Drag Reduction*, edited by G. R. Hough (American Institute of Aeronautics and Astronautics, New York, 1980), p. 290.

[25] P. G. De Gennes, "Towards a scaling theory of drag reduction," Physica A **140**, 9 (1986).

[26] G. Ryskin, "Turbulent drag reduction by polymers: A quantitative theory," Phys. Rev. Lett. **59**, 2059 (1987).